# Interface Dynamics of Strongly interacting Binary Superfluids

Yu-Ping An (安裕平)

Institute of Theoretical Physics, Chinese Academy of Sciences

7TH INTERNATIONAL CONFERENCE ON HOLOGRAPHY AND STRING THEORY IN DA NANG

Duy Tan University, Da Nang, Vietnam

23/08/2024

Based on arXiv:2401.09189(PRD), arXiv:2406.13965

Superfluidity, characterized by the flow of matter without resistance, represents a remarkable macroscopic quantum phenomenon observed in various systems, including ultracold atomic gases, liquid helium and strongly interacting high density matters existing inside neutron stars, and has broad applications.

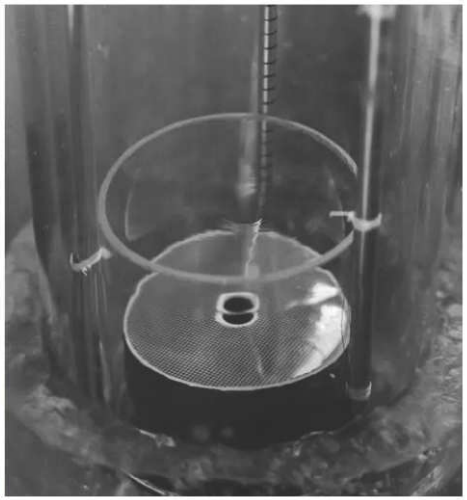

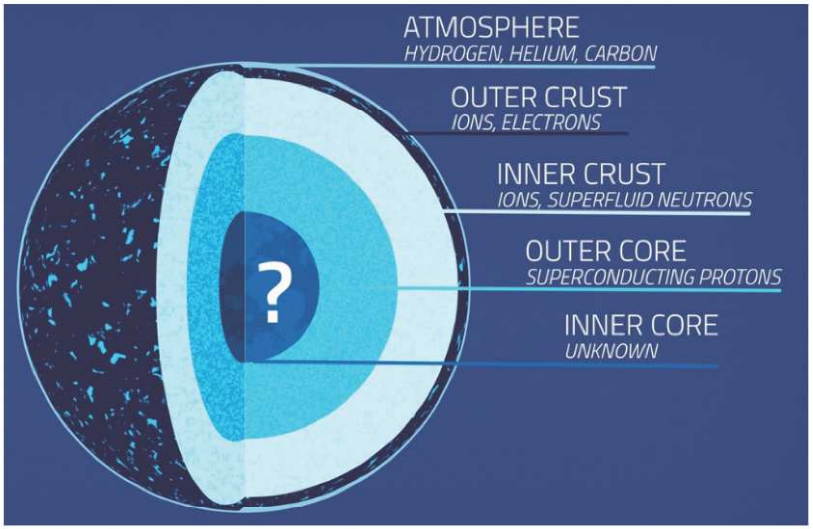

Some features of superfluid:

- Second order phase transition at critical temperature.
- Zero shear viscosity.
- Velocity field is irrotational $\nabla \times v_s = 0$.
- Quantized vortex.
- Landau critical velocity above which the superfluid becomes unstable.

The third and the fourth feature are consequences of the fact that order parameter of s-wave superfluids can be described by a complex scalar field $\mathcal{O} = \psi e^{i\theta}$ and $v_s = \nabla\theta$.

These features are all implemented by the simple holographic superfluid model:

$$S = \int dx^4 \sqrt{-g} \left[ \frac{1}{2\kappa_N^2} (R + \frac{6}{L^2}) + \mathcal{L}_m \right], \tag{1}$$

with

$$\mathcal{L}_m = -(\mathcal{D}_\mu \Psi)^* \mathcal{D}^\mu \Psi - m^2 |\Psi|^2 - \frac{1}{4} F^{\mu\nu} F_{\mu\nu}. \tag{2}$$

Various progress has be made based on this model, proving it to be a useful tool for exploring superfluid with dissipation and finite temperature effect at strong coupling limit.

## Quantum turbulence

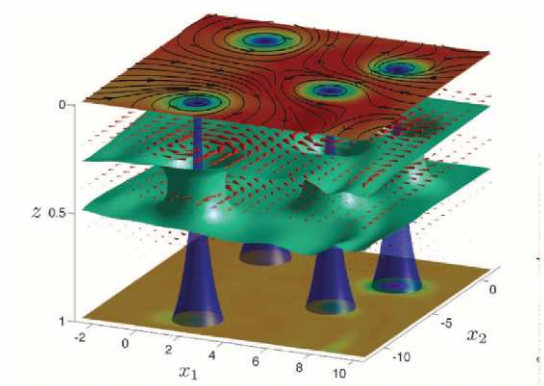

**Fig. 1. Holographic description of a superfluid with vortices.** The vertical axis is the radial direction $z$ of $AdS_4$. The planes $z = 0$ and $z = 1$ are the boundary of $AdS_4$ and the black hole horizon, respectively. The green surface is a surface of constant bulk charge density, with the region between the two slices defining a "slab" of condensate where most bulk charges reside. The slab screens excitations from falling into the horizon. This can be seen from the vector field (red arrows) indicating the energy flux $(-\tau^x_0, -\tau^y_0, -\tau^z_0)$ of Eq. 3, which vanishes rapidly below the slab. The vortices (blue tubes) punch holes through this screening slab, providing avenues for excitations to fall into the black hole. The surface $z = 0$ shows the condensate on the boundary (with blue representing zero condensate), superposed with flow lines of the superfluid velocity (Eq. 1). The $z = 1$ surface shows the flux of energy through the horizon. This energy flux is significant (red and green) only near the wake of the moving vortices, as is most easily seen in movies of the simulation available at http://turbulent.lns.mit.edu/Superfluid.

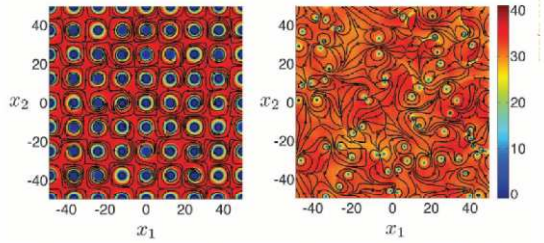

**Fig. 2. The superfluid condensate $|\langle\psi(t, x)\rangle|^2$ at time $t = 0$ (left) and $t = 300$ (right).** Flow lines of the superfluid current $\mathcal{J}(t, x)$ (defined in Eq. 1) are superimposed. The superfluid current circulates around the core of each vortex, where the condensate vanishes. The $W = \pm 6$ vortices (left) are much larger than the $W = \pm 1$ vortices (right). The yellow arcs seen in the right panel are waves produced by the annihilation of vortex pairs.

Paul M. Chesler et al. Science341,368-372(2013).

## Kibble-Zurek mechanism

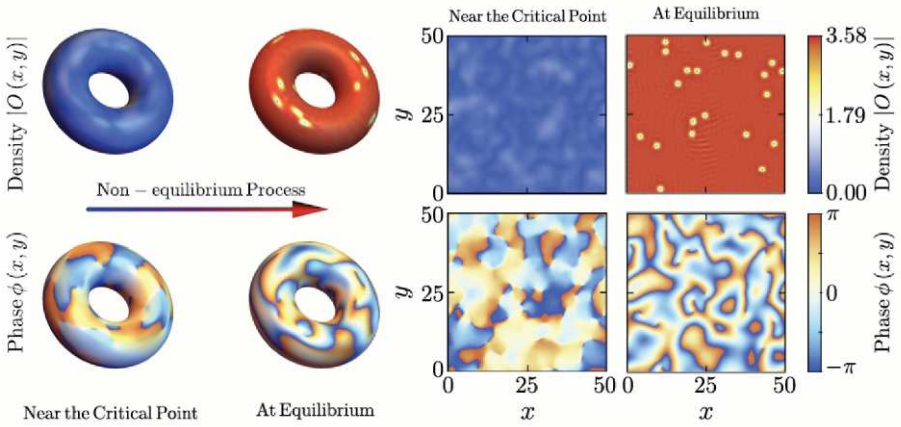


del Campo, A., Gómez-Ruiz, F.J., Li, ZH. et al. J. High Energ. Phys. 2021, 61 (2021).

## Energy cascade

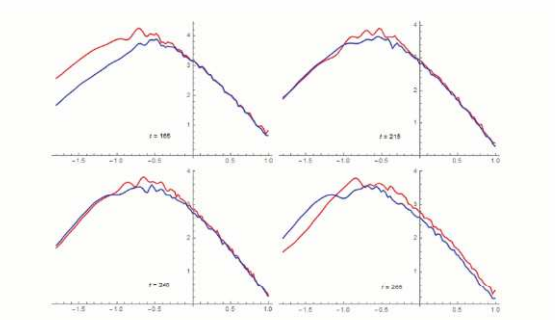

**Figure 7.** The comparison of the kinetic energy spectra $\epsilon_{kin}(t, k)$ at time $t = 165, 215, 240, 265$ between the driven and undriven systems. The external sources are turned on at $t = 150$ and turned off at $t = 210$. The blue curve is the kinetic energy spectrum for the undriven superfluid while the red one is that for the driven superfluid. The injected energy at the IR is propagating to UV.

Lan, S., Tian, Y. & Zhang, H. J. High Energ. Phys. 2016, 92 (2016).

## Vortex dynamics

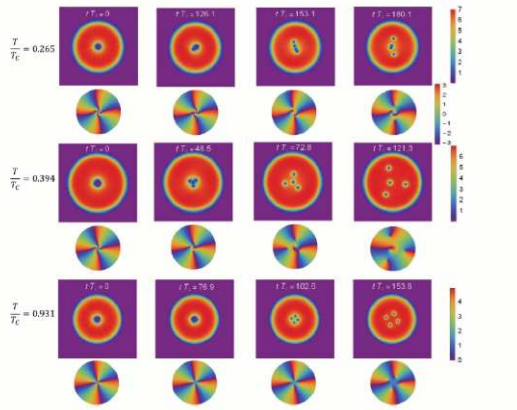


FIG. 3. Density and phase plots of the condensate for splitting processes of the quadruply quantized vortex under random perturbations with distinct splitting patterns at different temperatures.

Shanquan Lan, Xin Li, Yu Tian, Peng Yang, and Hongbao Zhang. Phys. Rev. Lett. 131, 221602

On the other hand, interface instabilities are ubiquitous in nature, found in both classical hydrodynamics and quantum superfluids. Typically, they occur when the two phase-separated fluid components have relative velocity across the interface. In this case, they are denoted as Kelvin-Helmholtz instability (KHI).

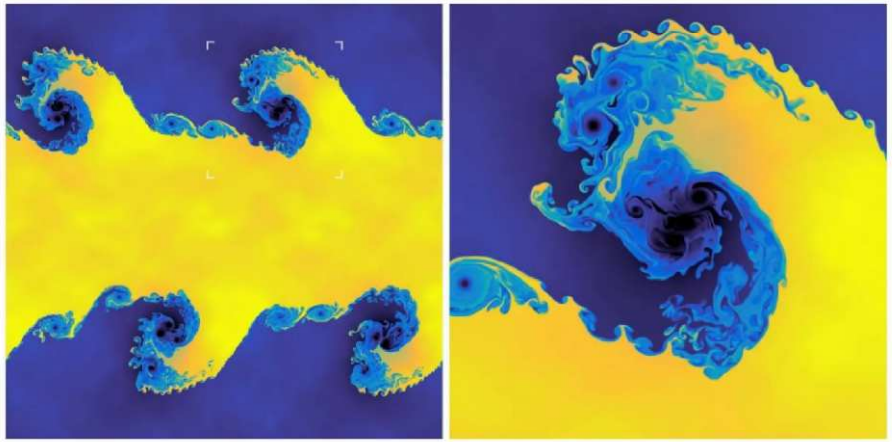

Figure taken from internet.

This phenomenon can also occur in quantum superfluids, called quantum Kelvin-Helmholtz instability (QKHI).

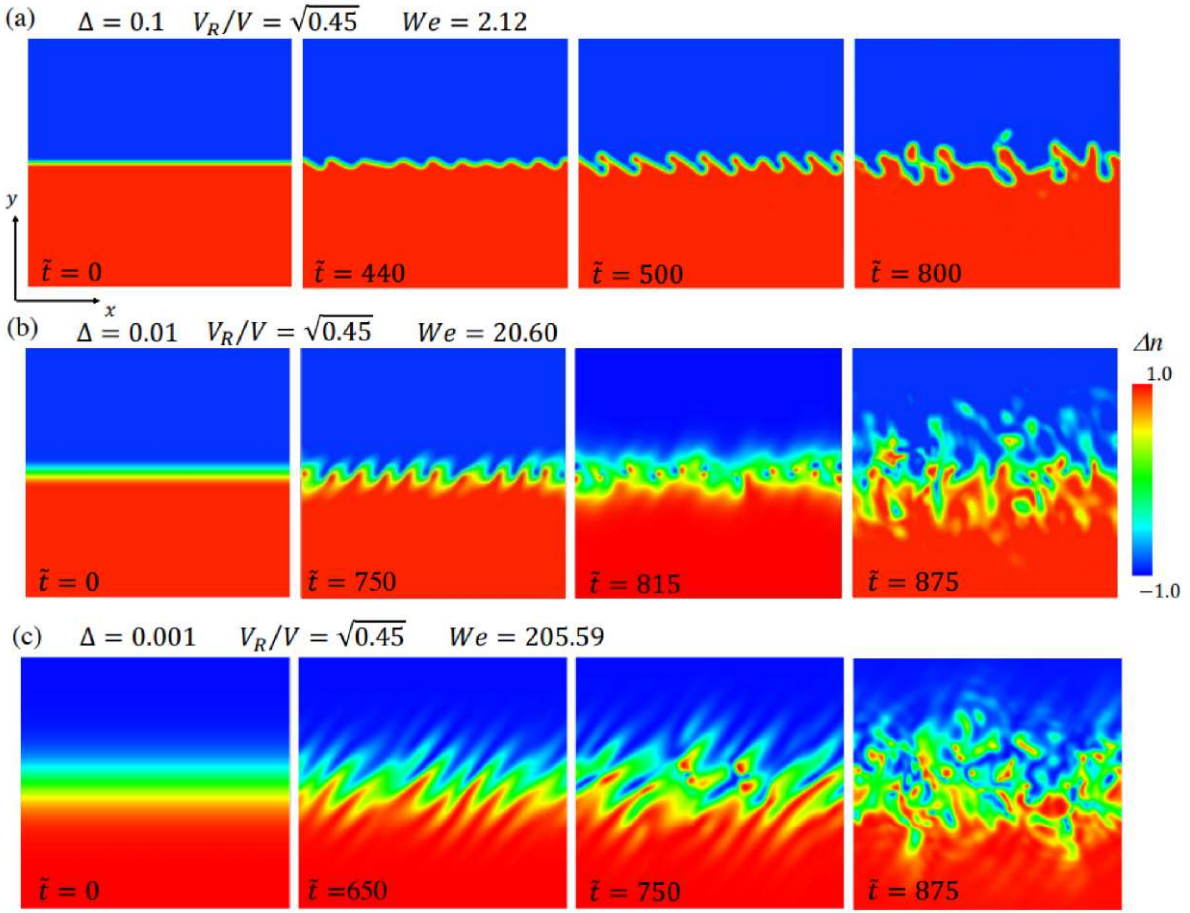


Figure taken from arXiv: 2104.13539.

Studies about QKHI usually rely on coupled Gross-Pitaevskii equation (GPE):

$$i\partial_t \Psi_i = (-\frac{1}{2m_i}\nabla^2 - \mu_i + g_i|\Psi_i|^2 + g_{ij}|\Psi_j|^2 + V_i)\Psi_i, \quad (i,j=1,2, \quad i \neq j). \tag{3}$$

which is a model equation for the ground-state single-particle wave-function in a weakly interacting Bose-Einstein condensate. $g_{12} > \sqrt{g_1 g_2}$ gives immiscible BECs, and $g_{12} < \sqrt{g_1 g_2}$ gives miscible ones.

However, this model does not include effects from dissipation and finite temperature, and it fails for strong interacting cases.

## Holographic setup

In this work we consider a 3+1 dimension holographic two-component superfluids model in probe limit. The Lagrangian for matter is:

$$\begin{aligned}\mathcal{L} = &-(\mathcal{D}_\mu\Psi_1)^*\mathcal{D}^\mu\Psi_1 - m_1^2|\Psi_1|^2 - (\mathcal{D}_\mu\Psi_2)^*\mathcal{D}^\mu\Psi_2 - m_2^2|\Psi_2|^2 \\ &- \frac{\nu}{2}|\Psi_1|^2|\Psi_2|^2 - \frac{1}{4}F^{\mu\nu}F_{\mu\nu},\end{aligned} \tag{4}$$

where $\mathcal{D}_\mu\Psi_i = (\nabla_\mu - ie_iA_\mu)\Psi_i$, $A_\mu$ is the $U(1)$ gauge field, $F_{\mu\nu}$ is the field strength and $\Psi_i$s are two complex scalar fields coupled with each other, so as to mimic interaction between two components of two-component superfluids.

As for background, we use a planar AdS black hole in Eddington-Finkelstein coordinates:

$$ds^2 = \frac{L^2}{z^2}(-(1-(z/z_h)^3)dt^2 - 2dtdz + dx^2 + dy^2). \tag{5}$$

For convenience, we set $L = z_h = 1$, $m_1^2 = m_2^2 = -2$, $e_1 = e_2 = 1$ and choose radial gauge $A_z = 0$, then asymptotic expansions for $A_\mu$ and $\Psi_i$ near AdS boundary read

$$\begin{aligned} A_\mu &= a_\mu + b_\mu z + \mathcal{O}(z^2), \\ \Psi_i &= (\Psi_i)_0 z + (\Psi_i)_1 z^2 + \mathcal{O}(z^3). \end{aligned} \tag{6}$$

From gauge-gravity duality, the coefficients $a_t$, $a_i$ $(i = x, y)$ and $(\Psi_i)_0$ can be interpreted as chemical potential $\mu$, vector potential, and scalar operator source at the boundary respectively. $(\Psi_i)_1$ corresponds to the expectation value of order parameter $\langle \mathcal{O} \rangle$.

## Stationary phase separated state

To study interface of two-component superfluids, we would like to find solutions which is homogeneous in y direction. Therefore, we can simplify EoMs by choosing the following ansatz:

$$\Phi_i = \phi_i(z,x)e^{i\theta_i(z,x,y)}, \quad A_t = A_t(z,x), \tag{7}$$

together with the gauge choice

$$\partial_z\theta_i = -\frac{A_t}{f}, \quad (v_i)_x = \partial_x\theta_i - A_x = 0, \quad (v_i)_y(z,x) = \partial_y\theta_i - A_y\,. \tag{8}$$

Consistence of above ansatz requires $\partial_z(A_y + (v_i)_y) = 0$.

EoMs reduce to

$$\partial_z(f\partial_z\phi_i) + \partial_x^2\phi_i - (v_i)_y^2\phi_i + \frac{A_t^2}{f}\phi_i - z\phi_i - \frac{\nu}{2}\phi_j^2\phi_i = 0, \tag{9}$$

$$f\partial_z^2 A_t + \partial_x^2 A_t - 2A_t(\sum_i \phi_i^2) = 0. \tag{10}$$

$$\partial_z(f\partial_z(v_i)_y) + \partial_x^2(v_i)_y - 2\sum_i (v_i)_y\phi_i^2 = 0. \tag{11}$$

We solve these equations numerically by Newton-Raphson method. In z direction, we use Chebyshev pseudo spectral method with following boundary conditions at $z = 0$

$$\phi_i(z=0) = 0, \quad A_t(z=0) = \mu, \quad (v_i)_y(z=0) = (-1)^{(i-1)}v_y/2, \tag{12}$$

and regular condition at $z = 1$, where $v_y$ is the relative velocity between the two components. In $x$ direction, we use fourth order finite difference scheme and Neumann boundary condition.

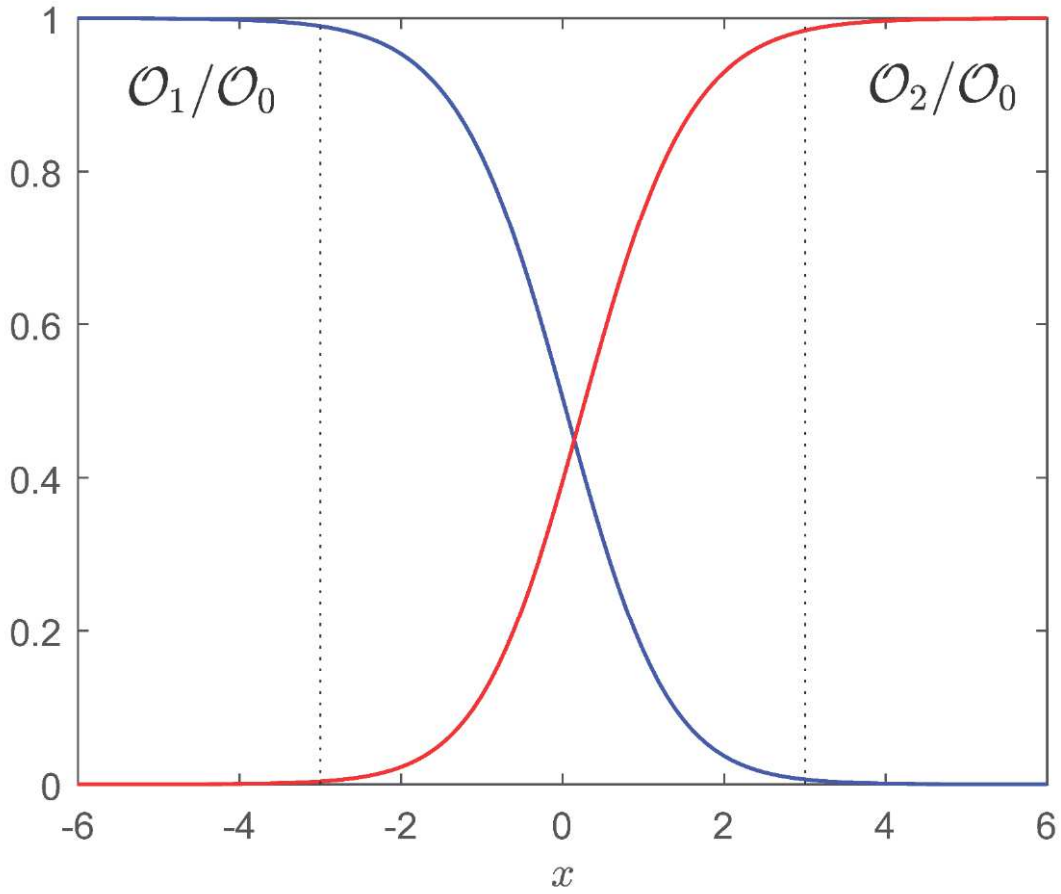


Figure 1: A typical stationary configuration for the immiscible binary superfluids. Plotted are the normalized order parameter of the two superfluid components $\mathcal{O}_i$ with $\mathcal{O}_0$ the value of the order parameter far from the interface. The phase with a interface consists of the configuration in which one component occupies half of the space and the other does the rest.

We can fit the profiles by

$$|\mathcal{O}_1|^2 = \frac{|\mathcal{O}_0|^2}{2}(1 - \tanh(x/\delta)), \tag{13}$$

where $\delta$ stands the width of the interface.

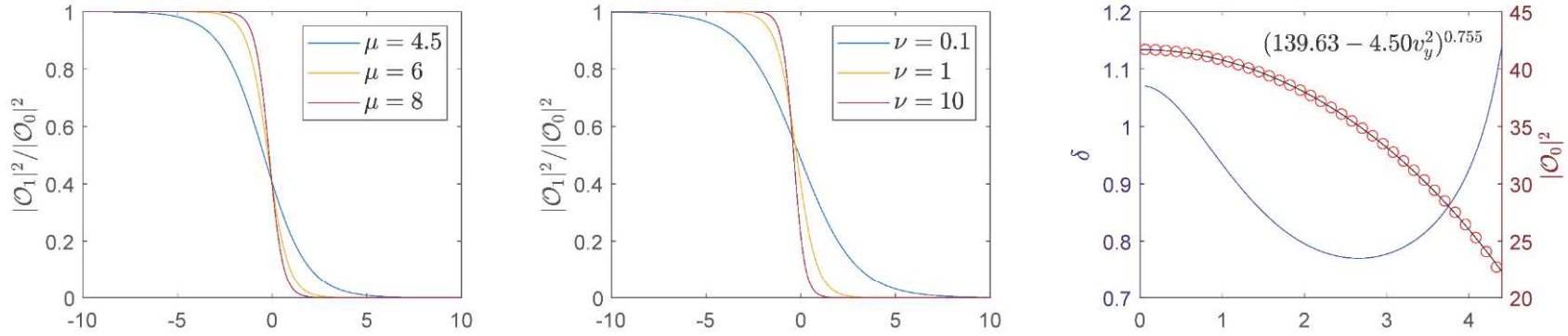


(a) Normalized $|\mathcal{O}_1|^2$ for different $\mu$; $\nu = 1$ and $v_y = 0$.

(b) Normalized $|\mathcal{O}_1|^2$ for different $\nu$; $\mu = 6$ and $v_y = 0$.

(c) Interface width $\delta$ and $|\mathcal{O}_0|^2$ for different $v_y$; $\mu = 6$ and $\nu = 1$.

Figure 2: Normalized order parameter of the first component for different $\mu$ and $\nu$, and interface width $\delta$ and $|\mathcal{O}_0|^2$ for different $v_y$. $\mathcal{O}_0$ is the value of the order parameter far from the interface. Profiles of $|\mathcal{O}_2|^2$ are mirror image of those of $|\mathcal{O}_1|^2$ about x-axis. Black line in (c) is fitting result.

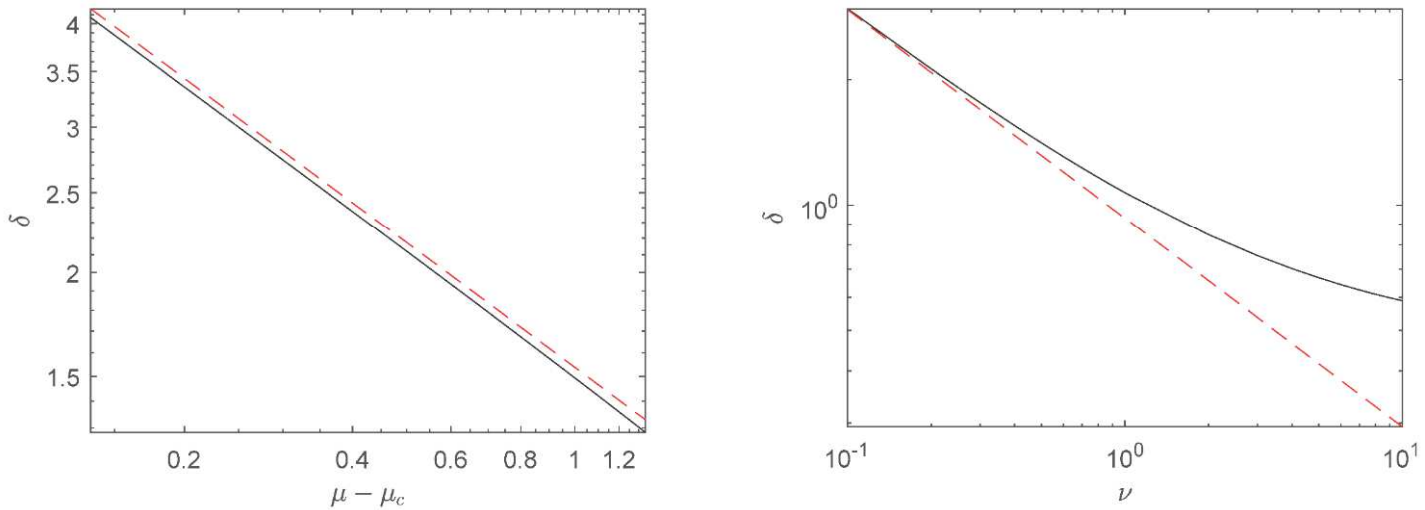


(a) $\delta - \mu$. $\nu = 1$. Slope of the dashed line is -0.5.

(b) $\delta - \nu$. $\mu = 6$. Slope of the dashed line is -0.5.

Figure 3: Interface width $\delta$ with different $\mu$ and $\nu$.

In GPE, when coupling strength $\Delta = g_{12}/g - 1$ is small, $\delta$ is given by $\delta = \xi/\Delta^{-1/2}$, where $\xi = \hbar/\sqrt{2m\mu}$ is the healing length. We see results from our holographic model is in agreement with those from GPE, if we identify $\mu - \mu_c$ and $\nu$ in holographic two-component superfluid model with $\mu$ and $\Delta$ in GPE.

# Dynamic instability

To observe the interface instability of two-component superfluids, we perturb the stationary configurations solved above. Since different initial conditions lead to quantitatively similar late-time patterns, we focus on initial condition of perturbed $\Phi_i$ that takes the following form:

$$\Phi_i = \Phi_{0i}[1 + \alpha \sum_k \exp(iky + i\theta_k)] \,, \tag{14}$$

where $\theta_k$ is a random phase for each $k$, and $\alpha$ is a small number which we set to be 0.01. The system is then evolved with this initial configuration for $\Phi_i$ while keeping the gauge field unperturbed.

We adopt the fourth order Runge-Kutta method along the time direction. At $z = 0$ the boundary conditions are

$$\Phi(z=0) = A_x(z=0) = A_y(z=0) = 0\,, \quad A_t(z=0) = \mu. \tag{15}$$

Thanks to the coordinate system we use, no boundary condition is imposed at the event horizon $z_h$. In the $y$ direction we use the period boundary condition with its size $L_y$, *i.e.*

$$\Phi(y) = \Phi(y + L_y), A_\mu(y) = A_\mu(y + L_y)\,. \tag{16}$$

We impose the Neumann boundary condition

$$\partial_x \Phi(x = \pm L_x/2) = \partial_x A_\mu(x = \pm L_x/2) = 0\,, \tag{17}$$

along the $x$ direction, with $L_x$ the size of the system. The size of our system $L_x \times L_y$ is prepared properly for each parameter set such that that the boundary effect can be negligible for the physics we are interested in.

When perturbation is turn on, phenomenons like quantum Kelvin-Helmholtz instability occur at the interface, just like what happens to two-component superfluid interface under perturbations from solving GPE.

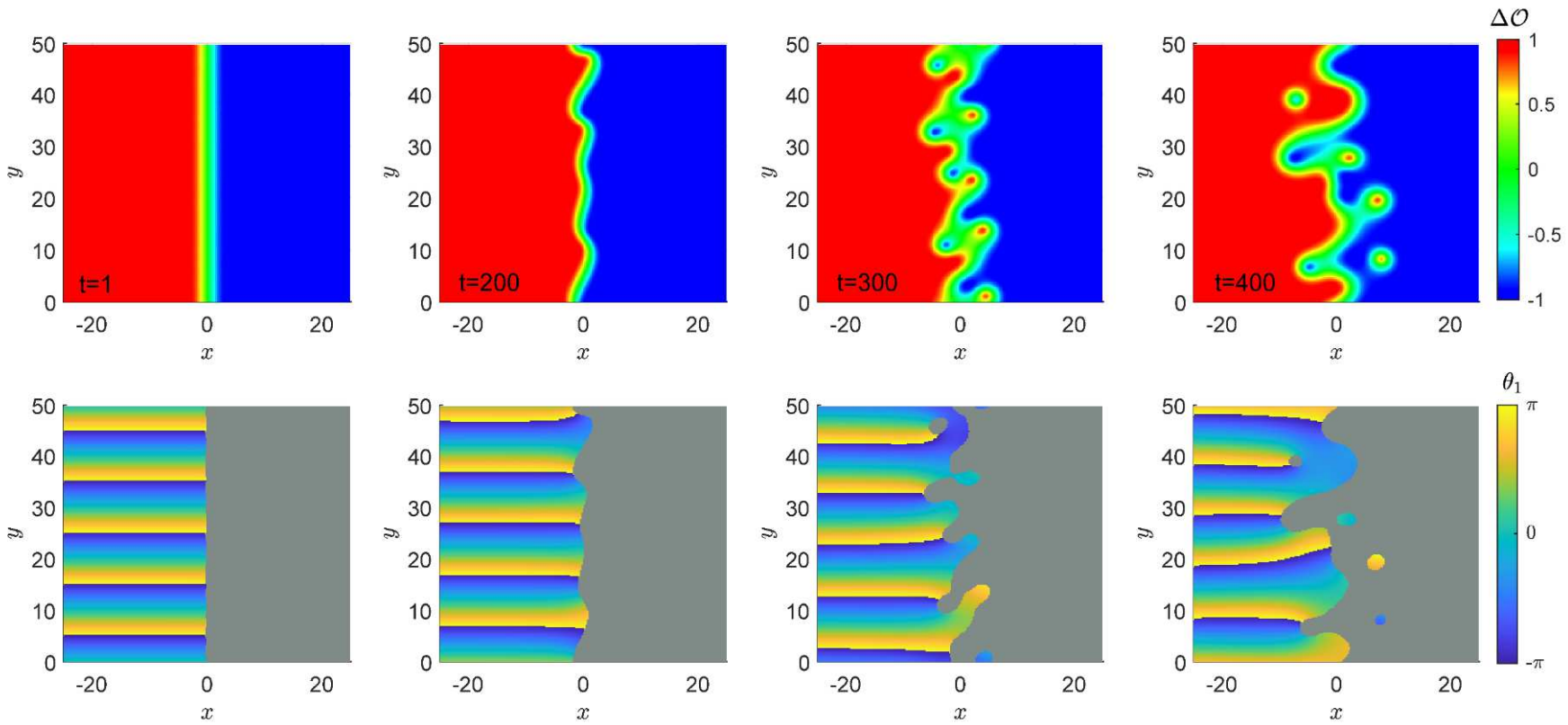


Figure 4: For $v_y = 1.2566$ at $T/T_c = 0.677$, snapshots of the condensation difference $\Delta\mathcal{O} = (|\mathcal{O}_1|^2 - |\mathcal{O}_2|^2)/|\mathcal{O}_0|^2$ **(upper panel)** and the profile of the phase of the first component $\theta_1$ **(bottom panel)** are presented at different times to illustrate the interface dynamics. Small initial perturbations on the interface destabilize and evolve into larger amplitude structures, leading to the formation of vortices and the onset of quantum turbulence. The plot of $\theta_1$ is restricted to cases where $|\mathcal{O}_1|^2 - |\mathcal{O}_2|^2 > 0$, as otherwise $|\mathcal{O}_1|$ is small, and $\theta_1$ would be dominated by noise. In this illustration, we set $\nu = 1$ and maintain $\mu = 6$.

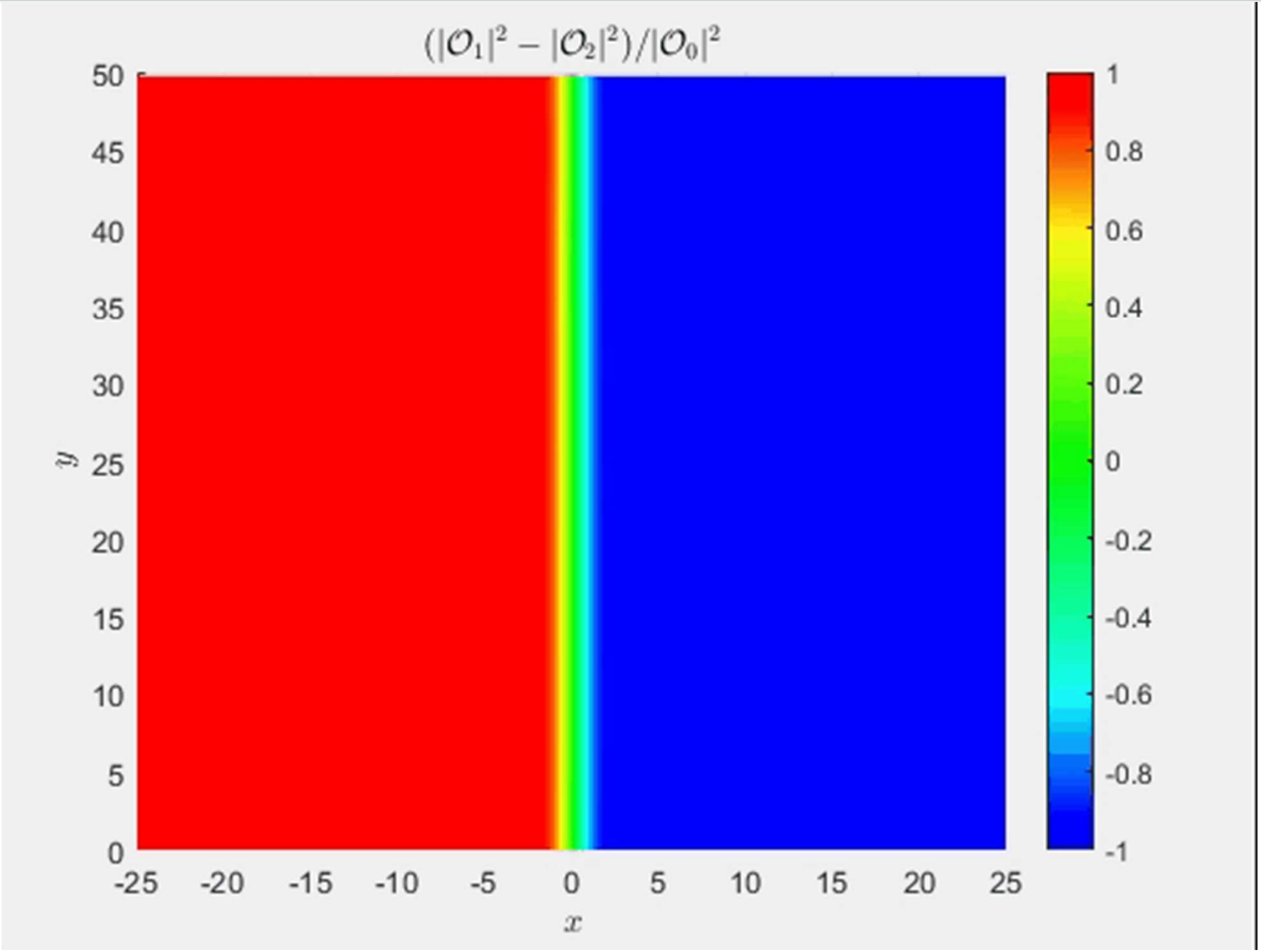
$(|\mathcal{O}_1|^2 - |\mathcal{O}_2|^2)/|\mathcal{O}_0|^2$
50
45
40
35
30
25
20
15
10
5
0
$y$
-25
-20
-15
-10
-5
0
5
10
15
20
25
$x$
1
0.8
0.6
0.4
0.2
0
-0.2
-0.4
-0.6
-0.8
-1

The onset of the instability of such stationary solutions can be analyzed by the linear response theory. We turn on the linear perturbations on the stationary background

$$\begin{aligned} \Phi_i &= \Phi_{i0} + \delta\Phi_i, \quad A_t = A_{t0} + \delta A_t, \\ A_x &= A_{x0} + \delta A_x, \quad A_y = A_{y0} + \delta A_y \,, \end{aligned} \tag{18}$$

where $\Phi_{0i}$, $A_{t0}$, $A_{x0}$ and $A_{y0}$ are stationary solutions. Considering the fact that the background is the same over time and in the $y$-direction, we choose the bulk perturbation fields as:

$$\begin{aligned} &\delta\Phi_i = u_i(z,x)e^{-i(\omega t - ky)}e^{i(v_i)_y y}, \quad \delta\Phi_i^* = v_i(z,x)e^{-i(\omega t-ky)}e^{-i(v_i)_y y}, \\ &\delta A_t = a_t(z,x)e^{-i(\omega t-ky)}, \quad \delta A_x = a_x(z,x)e^{-i(\omega t-ky)}, \quad \delta A_y = a_y(z,x)e^{-i(\omega t-ky)}. \end{aligned} \tag{19}$$

The resulting linear perturbation equations are

$$
\begin{aligned}
&2iA_{t0}\partial_z u_i + 2ia_t\partial_z\Phi_{0i} + i\partial_z A_{t0}u_i + i\partial_z a_t\Phi_{0i} + \partial_z(f\partial_z u_i) - zu_i + \partial_x^2 u_i - (k+(v_i)_y)^2 u_i - i\partial_x A_{x0}u_i \\
&- i\Phi_{0i}(\partial_x a_x + ika_y) - (A_{x0}^2 + A_{y0}^2)u_i - 2A_{x0}\Phi_{0i}a_x - 2A_{y0}\Phi_{0i}a_y - 2i(A_{x0}\partial_x u_i + i(k+(v_i)_y)A_{y0}u_i) \\
&- 2i(a_x\partial_x\Phi_{0i} + ia_y(v_i)_y\Phi_{0i}) - \frac{\nu}{2}|\Phi_{0j}|^2 u_i - \frac{\nu}{2}\Phi_{0j}^*\Phi_{0i}u_j - \frac{\nu}{2}\Phi_{0j}\Phi_{0i}v_j \\
&= -2i\omega\partial_z u_i, \qquad (i,j=1,2 \quad i\neq j)\,, \\
&- 2iA_{t0}\partial_z v_i - 2ia_t\partial_z\Phi_{0i}^* - i\partial_z A_{t0}v_i - i\partial_z a_t\Phi_{0i}^* + \partial_z(f\partial_z v_i) - zv_i + \partial_x^2 v_i - (k-(v_i)_y)^2 v_i + i\partial_x A_{x0}v_i \\
&+ i\Phi_{0i}^*(\partial_x a_x + ika_y) - (A_{x0}^2 + A_{y0}^2)v_i - 2A_{x0}\Phi_{0i}^*a_x - 2A_{y0}\Phi_{0i}^*a_y + 2i(A_{x0}\partial_x v_i + i(k-(v_i)_y)A_{y0}v_i) \\
&+ 2i(a_x\partial_x\Phi_{0i}^* - ia_y(v_i)_y\Phi_{0i}^*) - \frac{\nu}{2}|\Phi_{0j}|^2 v_i - \frac{\nu}{2}\Phi_{0j}\Phi_{0i}^*v_j - \frac{\nu}{2}\Phi_{0j}^*\Phi_{0i}^*u_j \\
&= -2i\omega\partial_z v_i, \qquad (i,j=1,2 \quad i\neq j)\,, \\
&\partial_x^2 a_t - k^2 a_t + f\partial_z\partial_x a_x + ikf\partial_z a_y - 2a_t\sum_i|\Phi_{0i}|^2 - 2A_{t0}\sum_i(\Phi_{0i}^*u_i + \Phi_{0i}v_i) + if\sum_i(\Phi_{0i}^*\partial_z u_i \\
&- \Phi_{0i}\partial_z v_i + v_i\partial_z\Phi_{0i} - u_i\partial_z\Phi_{0i}^*) = -i\omega(\partial_z a_t + \partial_x a_x + ika_y) + \omega\sum_i(\Phi_{0i}^*u_i - \Phi_{0i}v_i)\,, \\
&\partial_z(\partial_x a_t + f\partial_z a_x) - (k^2 a_x + ik\partial_x a_y) - 2a_x\sum_i|\Phi_{0i}|^2 - 2A_{x0}\sum_i(\Phi_{0i}^*u_i + \Phi_{0i}v_i) \\
&- i\sum_i(\Phi_{0i}^*\partial_x u_i - \Phi_{0i}\partial_x v_i + v_i\partial_x\Phi_{0i} - u_i\partial_x\Phi_{0i}^*) = -2i\omega\partial_z a_x, \\
&ik\partial_z a_t + \partial_z(f\partial_z a_y) + \partial_x^2 a_y - ik\partial_x a_x - 2a_y\sum_i|\Phi_{0i}|^2 - 2A_{y0}\sum_i(\Phi_{0i}^*u_i + \Phi_{0i}v_i) \\
&+ \sum_i((k+(v_i)_y)\Phi_{0i}^*u_i - (k-(v_i)_y)\Phi_{0i}v_i + (v_i)_y v_i\Phi_{0i} + (v_i)_y u_i\Phi_{0i}^*) = -2i\omega\partial_z a_y\,.
\end{aligned}
$$

This results in a generalized eigenvalue problem

$$M_k u_k = i\omega_k B u_k, \quad u_k = \{u_1, v_1, u_2, v_2, a_t, a_y\}_k^{\mathrm{T}}. \tag{20}$$

Since $\delta\Phi \sim e^{-i\omega t}$, the stationary configuration is dynamical unstable whenever $\mathrm{Im}\omega_k > 0$.
Note that the complex conjugates of linearized equations of motion can be obtained via the following transformation:

$$k \to -k, \quad \omega \to -\omega^*, \quad u_i \leftrightarrow v_i^*, \quad a_\mu \to a_\mu^*, \tag{21}$$

so that whenever $\omega$ is an eigenvalue for given wave number $k$, $-\omega^*$ is an eigenvalue for $-k$, and they share the same imaginary part. Therefore, without loss of generality, we only need to consider positive $k$.

To gain the quantitative feature of the system, we consider the wave number of the most unstable modes $k_0$ versus the relative velocity $v_y$. From linear analysis, for each velocity, the imaginary part rises with the increase of $k$, peaks at a certain wave number that corresponds to the most unstable mode $k_0$.

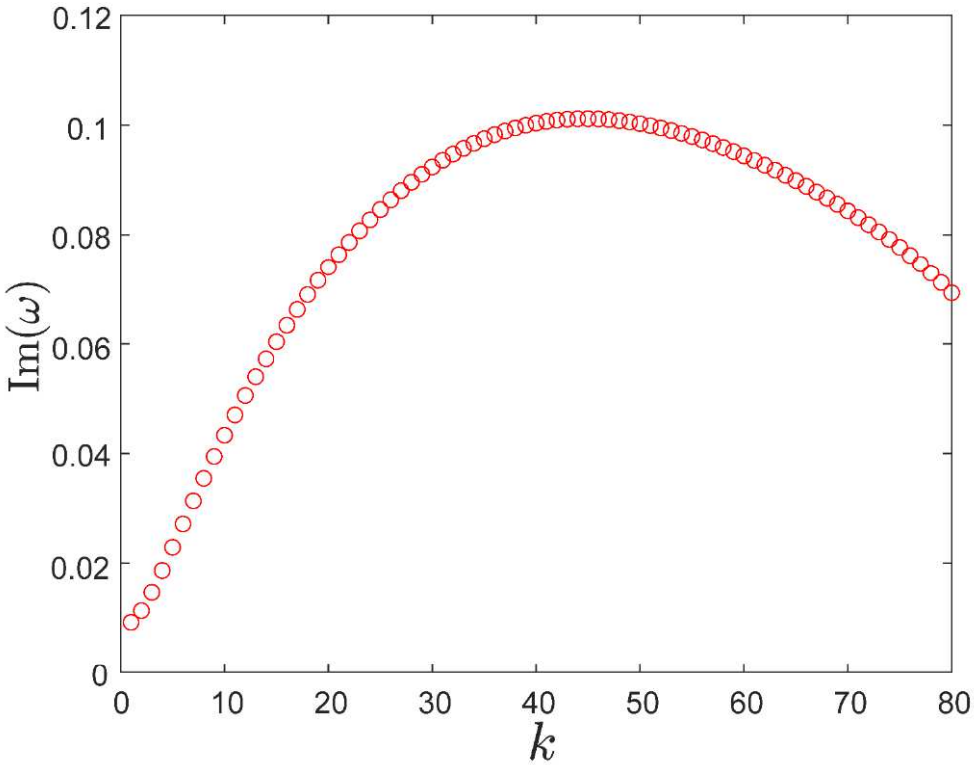


Figure 5: The largest imaginary of the spectrum of QNMs of stationary configurations with $T/T_c = 0.677$ and $v_y = 2.5132$. We fix $\nu = 1$ and $\mu = 6$.

From time evolution, we extract Fourier spectrum of the shape of interface at each time before the vortices develop. For each $v_y$, we find a stable peak in Fourier spectrum at $k_0$ during non-linear evolution.

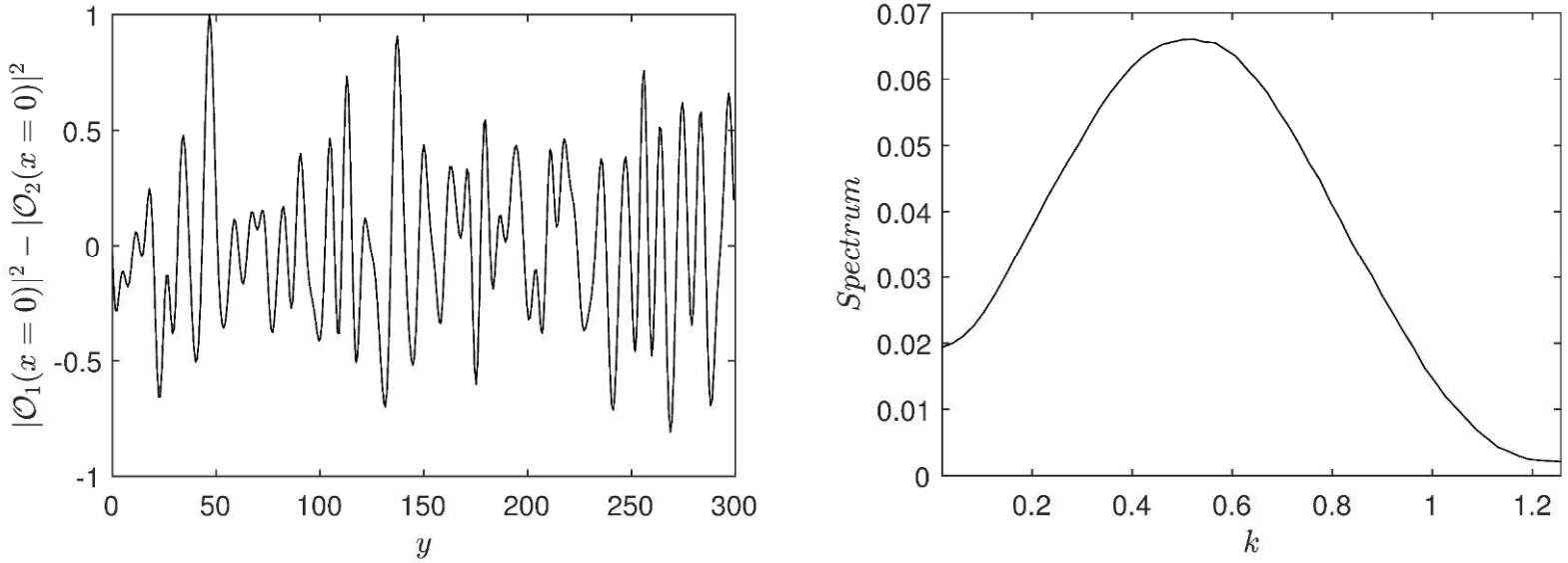


Figure 6: **Left panel**: $|\mathcal{O}_1|^2 - |\mathcal{O}_2|^2$ at $x = 0$. **Right panel**: Fourier transforms of the shapes of interface.

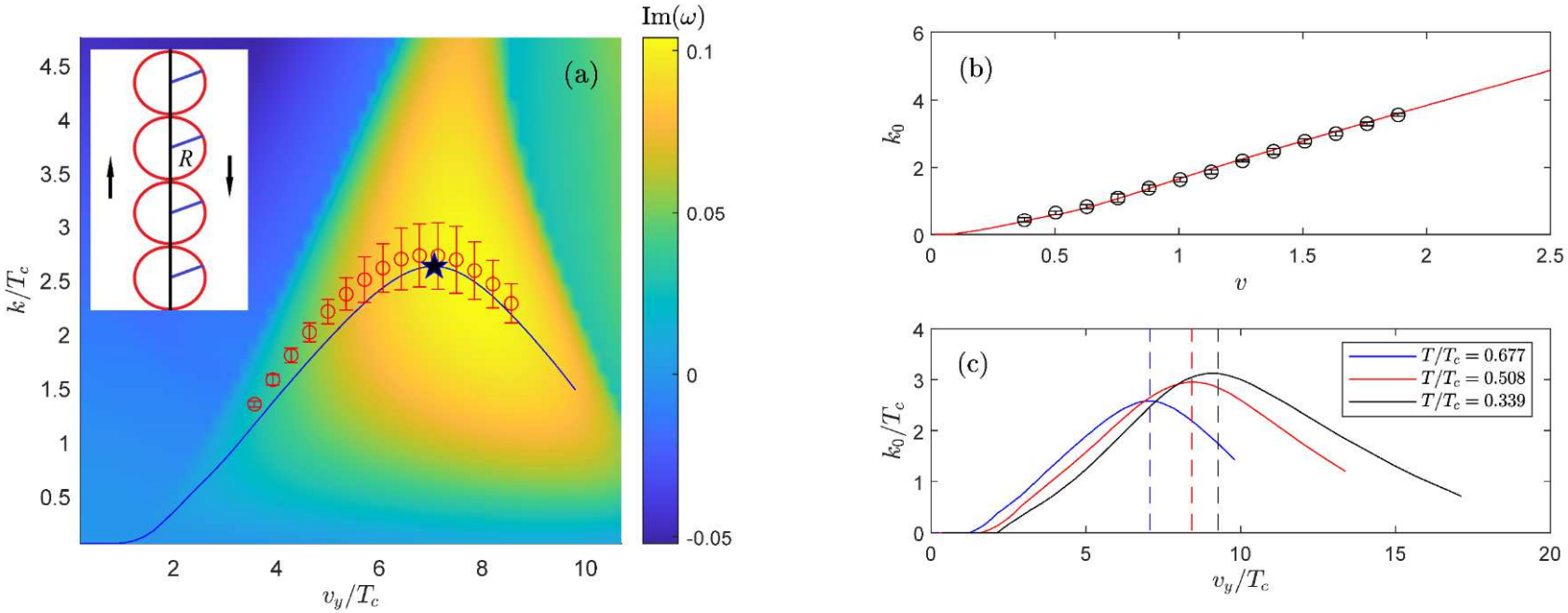


**Figure 7:** **(a)** The plot depicts the wave number of the fastest-growing mode $k_0$ as a function of interfacial relative velocity for $T/T_c = 0.677$. The circles with error bars represent $k_0$ values extracted from real-time evolution, while the solid line corresponds to perturbation analysis around the stationary state. The density plot provides information on the dominant Quasinormal Modes (QNMs) for each combination of wave number and velocity. The **insert** illustrates the highest point (star) where the average distance of vortices $4\pi/v_y$ equals the vortex size $2R$. **(b)** Displays the $k_0$ vs. $v$ relation according to the Gross-Pitaevskii equation (GPE) at zero temperature. **(c)** Illustrates $k_0 - v$ the relation from our holographic theory at various temperatures. Dashed vertical lines indicate critical velocities where the average distance of vortices generated along the interface equals the vortex size. The parameter is chosen to be $\nu = 1$.

# Coflow instability

When wind blows through flags, flags would flap, showing instability. The flag acts like a interface between the wind aside it, and the wind in the two sides are flowing with the same velocity in the same direction. What about interface of binary superfluids?

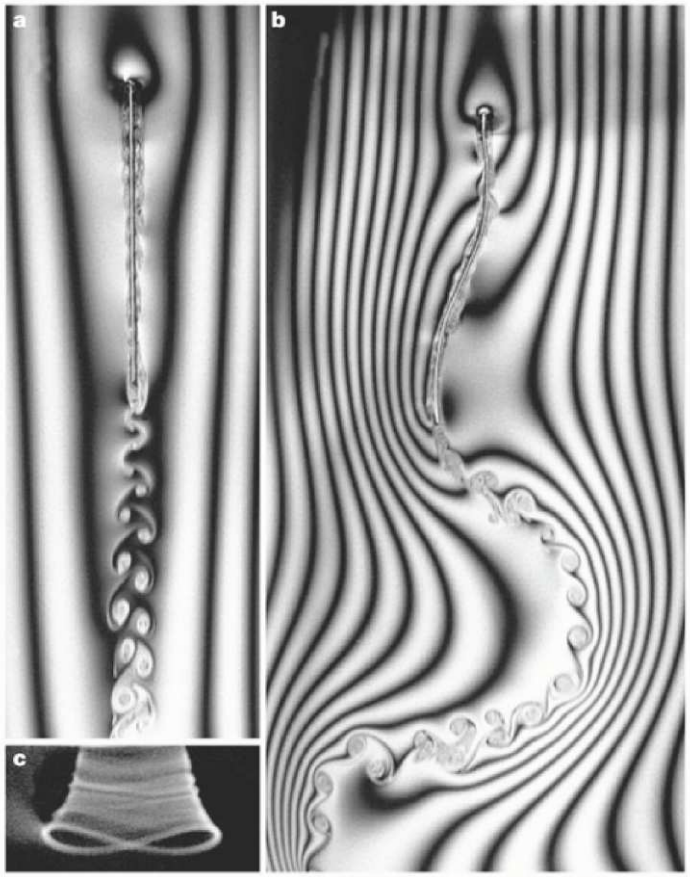


**Figure 2** The two stable states of the filament. When the filament length is greater than the critical value, it can stay in either a stretched-straight state or an oscillatory state. The flow is visualized using interference patterns under a sodium lamp. **a**, The filament is stretched straight in the flow. Von Kármán type vortices are shed from its free end. **b**, The oscillatory flapping state. Flow structures, modulated by the filament, are advected downstream. Interference fringes run in the flow direction, indicating that the soap film is under little stretching and compression. **c**, The free end of the filament shows a 'figure of eight' trajectory owing to the existence of the travelling waves associated with the flapping motion.

Zhang, J., Childress, S., Libchaber, A. et al. Nature 408, 835–839 (2000).

At finite temperature, a superfluid and a normal fluid component coexist. The interface of the binary superfluids could be unstable due to the relative velocity between the superfluid component and normal component. This can not be presented by GPE due to its Galilean invariant nature.

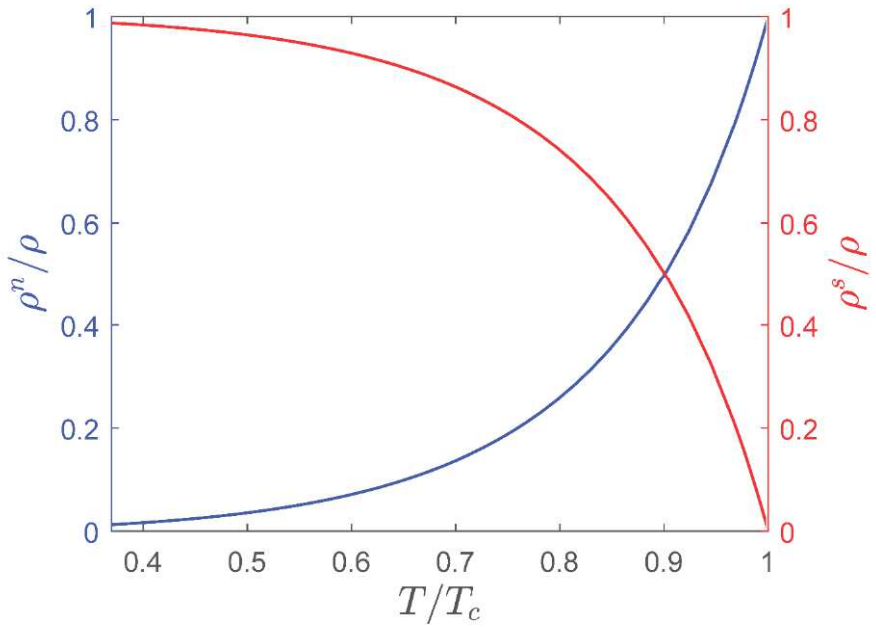


Figure 8: The fraction $\rho^s/\rho$ carried by the superfluid condensate and the one $\rho^n/\rho$ by the normal fluid component as a function of temperature, where $\rho = \rho^s + \rho^n$.

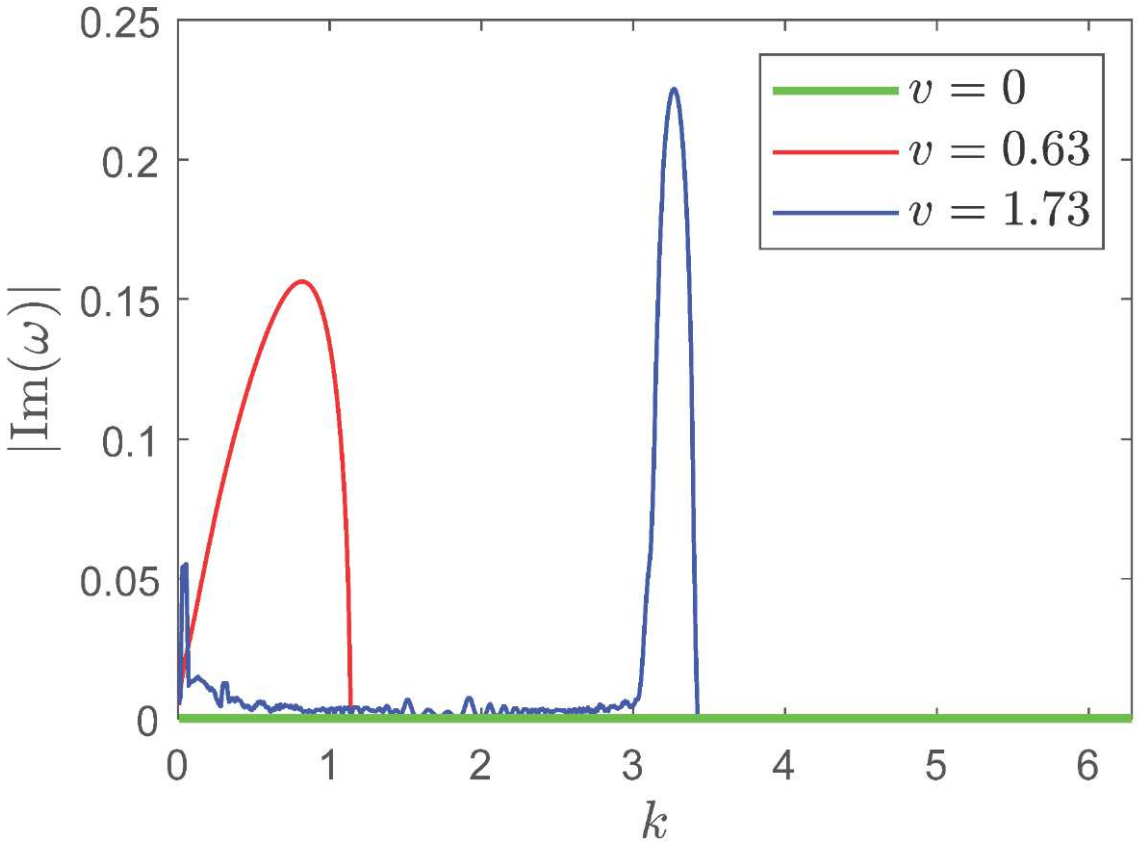


Figure 9: $|\mathrm{Im}(\omega)|$ versus $k$ for superflow velocity $v_1^s = -v_2^s = v$ obtained from the GPEs. The system becomes dynamically unstable whenever $\mathrm{Im}(\omega) \neq 0$. Green, red and blue lines correspond to $v = 0$, $0.63$ and $1.73$, respectively. It is manifest that there is no instability for $v = 0$. We have chosen $g = m = 1$, $g_{12} = 2$ and $\mu = 0.5$.

Dissipation or finite temperature effect in GPE is often considered by adding a phenomenological dissipation term:

$$i\partial_t\Psi_i \to i\partial_t\Psi_i - \gamma\partial_t\Psi_i\,, \tag{22}$$

with $\gamma$ a constant. The effect of this additional parameter $\gamma$ to $\omega$ is simply

$$\omega \to \omega' = (1 - i\gamma)\omega\,. \tag{23}$$

This leads to nonphysical effect of co-flow instability. That is, at large momentum, instability strength increases unboundedly as $k$ increases. Compared to this naive phenomenological model, the holographic model gives more natural and physical result.

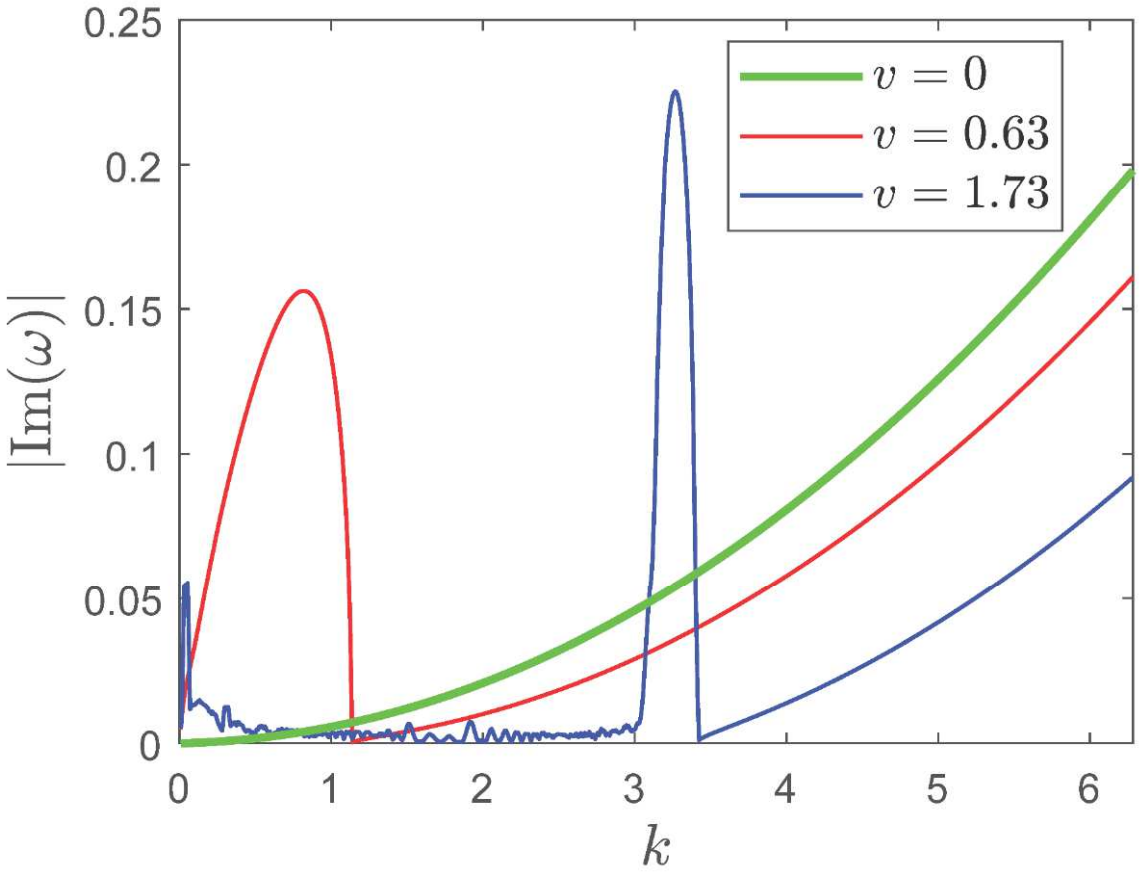


Figure 10: The same quantities are shown as in Fig. 9 with the same parameters, except that additional dissipation $\gamma = 0.01$ is included. This gives nonphysical result for co-flow interface instability: instability strength grows fast and unboundedly as $k$ increases.

Due to relative velocity between superfluid component and normal component, interface instability shows in our holographic model even the two superfluid components are flowing in the same direction with the same velocity. This is a quantum analog to the flapping of flags in wind, where the role of flag is played by the interface.

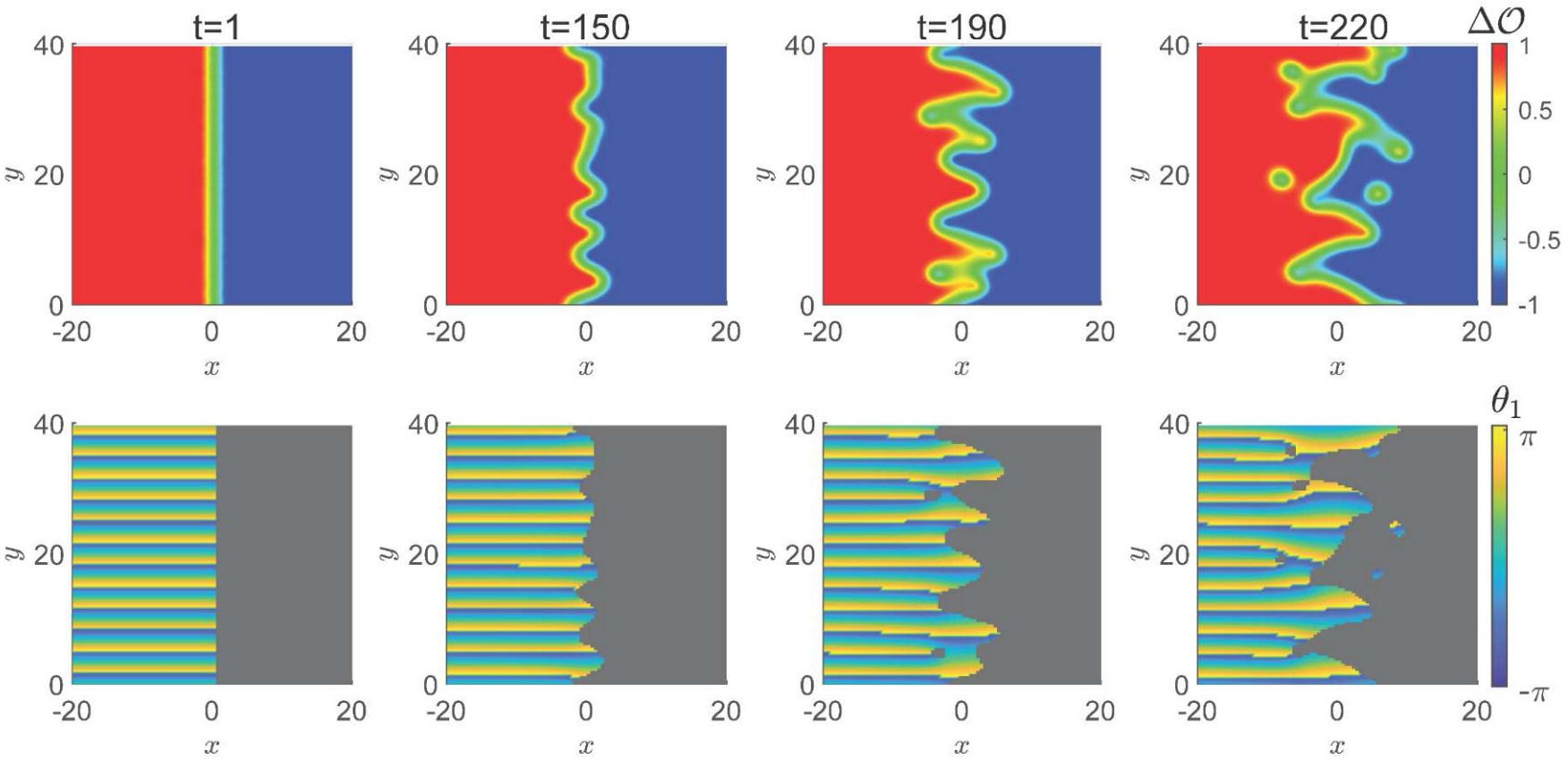


Figure 11: For $v_y/T_c = 5.348$ at $T/T_c = 0.677$, snapshots of the condensation difference $\Delta\mathcal{O} = (|\mathcal{O}_1|^2 - |\mathcal{O}_2|^2)/|\mathcal{O}_0|^2$ **(upper panel)** and the profile of the phase of the first component $\theta_1$ **(bottom panel)** are presented at different times to illustrate the interface dynamics. In this illustration, we set $\nu = 1$ and maintain $\mu = 6$.

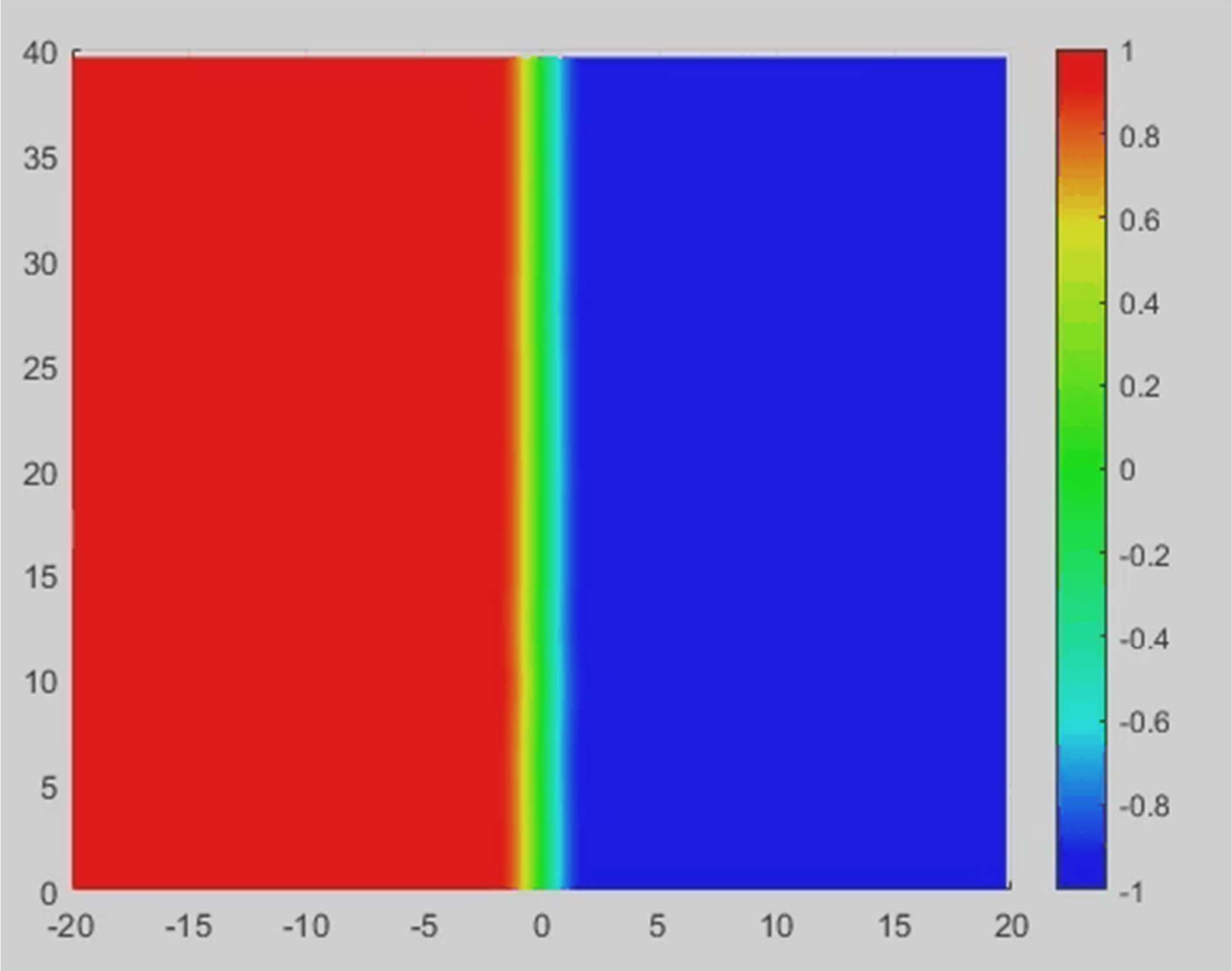
40
35
30
25
20
15
10
5
0
-20
-15
-10
-5
0
5
10
15
20
1
0.8
0.6
0.4
0.2
0
-0.2
-0.4
-0.6
-0.8
-1

Still, we can do linear analysis for this finite temperature interface instability. We can see for the case with zero relative velocity, $k_0 - v_y$ curve has no turning point and is monotonically increasing with respect to overall velocity $v_y$. For fixed velocity, $k_0$ and the overall instability decrease as temperature decrease, which is expected since normal component should disappear as temperature goes to 0.

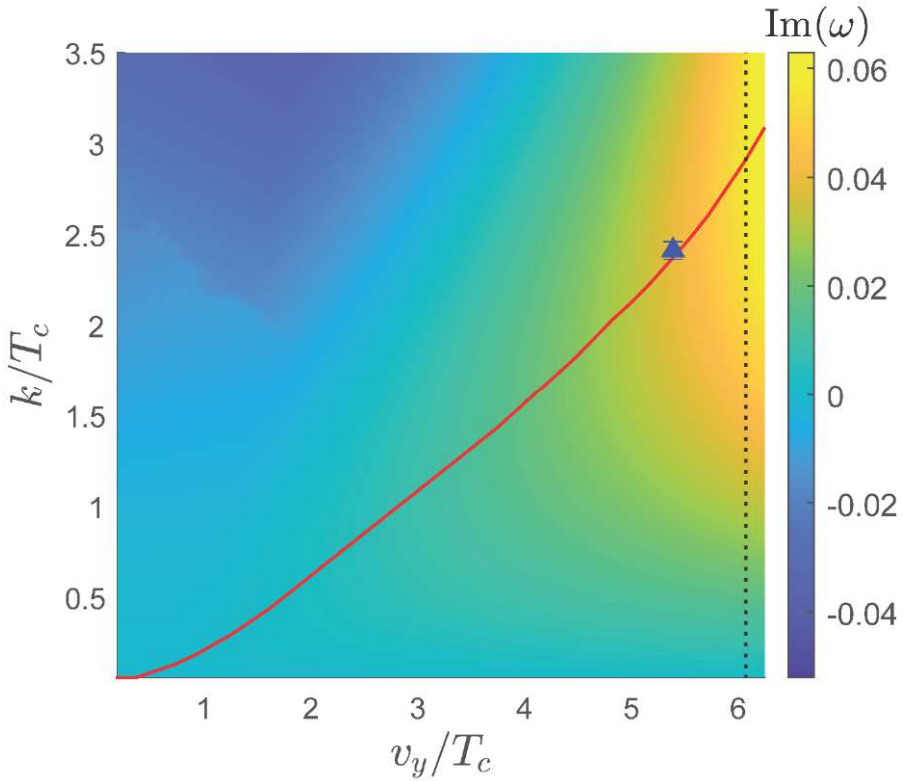


Figure 12: Illustration for the dynamical interface instability via QNMs around the stationary phase-sperated configuration with $T/T_c = 0.677$ and $\nu = 1$. The density plot shows $\mathrm{Im}(\omega)$ in terms of $k$ and $v_y$ with $T/T_c = 0.677$ for which the fastest growing modes are denoted by the red curve. The blue triangle corresponds to $k_0$ extracted from time evolution at the same velocity as in Fig. 11. The black vertical dashed line denotes the critical velocity $v/T_c = 6.06$ beyond which the Landau instability begins to appear.

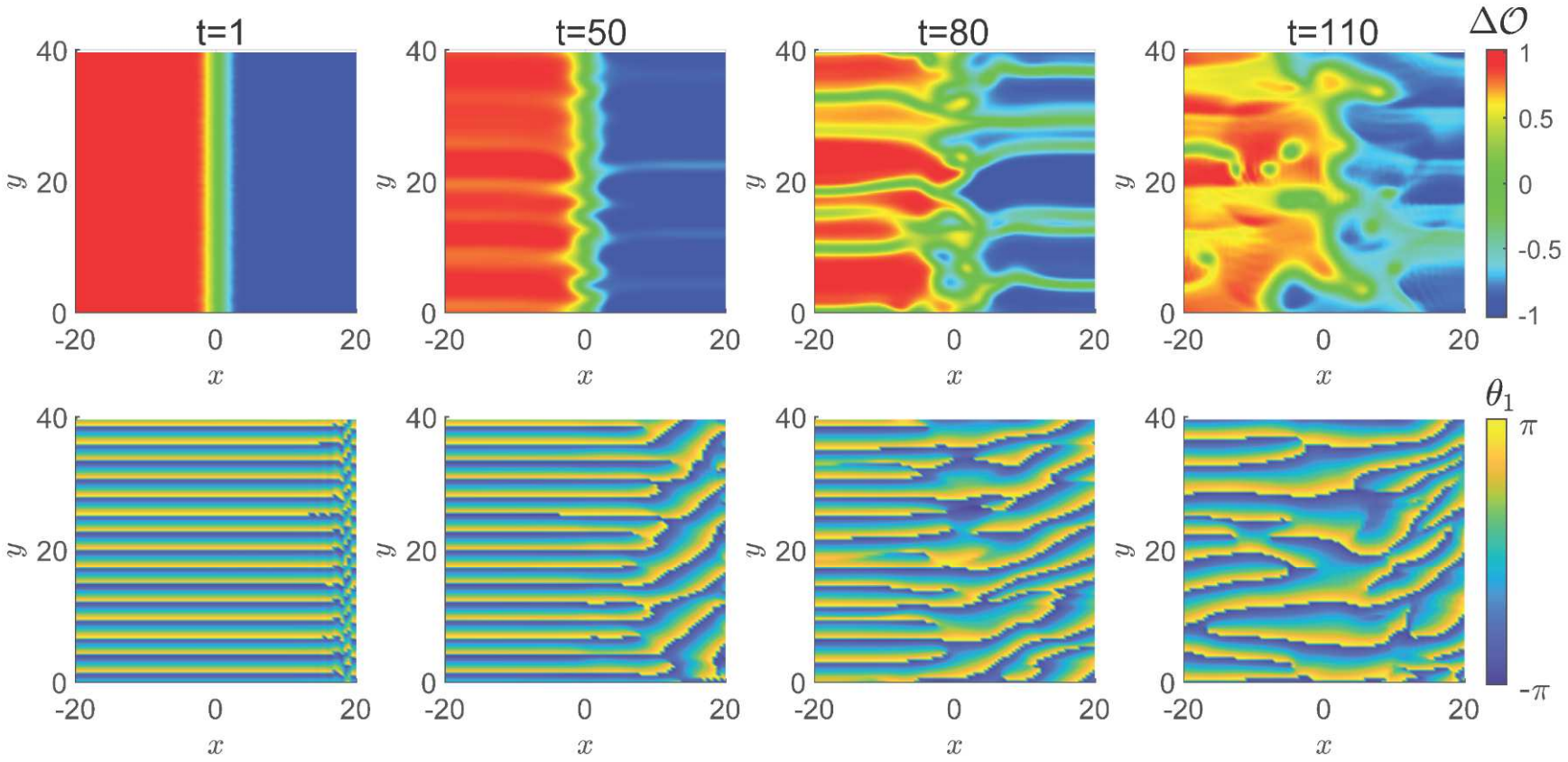


Figure 13: Interface patterns for two superfluid components moving beyond the Landau critical velocity. For $v_y/T_c = 6.685$ at $T/T_c = 0.677$, snapshots of the condensation difference $\Delta\mathcal{O} = (|\mathcal{O}_1|^2 - |\mathcal{O}_2|^2)/|\mathcal{O}_0|^2$ **(upper panel)** and the profile of the phase of the first component $\theta_1$ **(bottom panel)** are presented at different times to illustrate the interface dynamics. In this illustration, we set $\nu = 1$ and maintain $\mu = 6$.

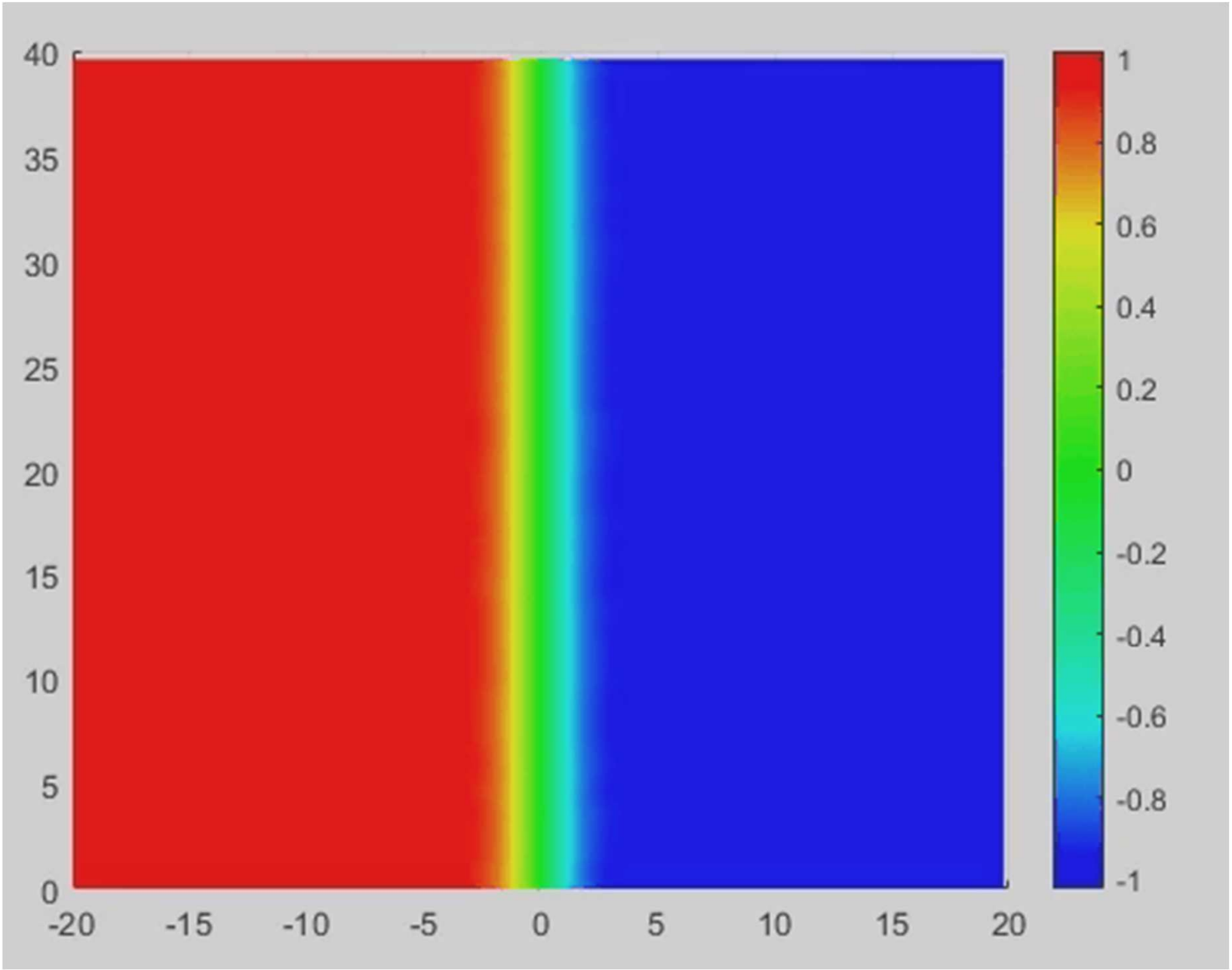
40
35
30
25
20
15
10
5
0
-20
-15
-10
-5
0
5
10
15
20
1
0.8
0.6
0.4
0.2
0
-0.2
-0.4
-0.6
-0.8
-1

# Summary:

- Our work initiates the investigation of interface instabilities in the holography laboratory, providing an intriguing platform to explore the interplay of instabilities and the emergence of complex flow phenomena.
- For counterflow case, from both the far-from-equilibrium evolution and the linear QNMs analysis, we find that the $k_0$ depends non-monotonically on the superfluid velocity. We have uncovered that the turning point occurs when the mean separation of vortices generated by interface instabilities becomes comparable to the size of vortices, suggesting that the non-monotonicity is due to the direct interaction between neighbor vortices.
- We also give the first explicit realization of co-flow interface instability in quantum fluids, which is due to relative velocity between superfluid component and normal component.

## More coming and stay updated!

- Symbiotic vortex-bright soliton in immiscible binary superfluids.
- Instability in miscible binary superfluids.
- Composite vortex in miscible binary superfluids.